SERBIAN JOURNAL OF ELECTRICAL ENGINEERING
Vol. 8, No. 2, May 2011, 127-146

UDK: 629.313.65

The Efficiency of Direct Torque Control for Electric Vehicle Behavior Improvement

Brahim Gasbaoui[1], Abdelkader Chaker[2], Abdellah Laoufi[1], Boumediène Allaoua[1], Abdelfatah Nasri[1]

Abstract: Nowadays the electric vehicle motorization control takes a great interest of industrials for commercialized electric vehicles. This paper is one example of the proposed control methods that ensure both safety and stability the electric vehicle by the means of Direct Torque Control (DTC). For motion of the vehicle the electric drive consists of four wheels: two front ones for steering and two rear ones for propulsion equipped with two induction motors, due to their lightweight simplicity and high performance. Acceleration and steering are ensured by the electronic differential, permitting safe and reliable steering at any curve. The direct torque control ensures efficiently controlled vehicle. Electric vehicle direct torque control is simulated in MATLAB SIMULINK environment. Electric vehicle (EV) demonstrated satisfactory results in all type of roads constraints: straight, ramp, downhill and bends.

Keywords: Electric vehicle, Electronic differential, Induction motor, Direct torque control, Traction control.

1 Introduction

Today, automobile transportation is in a crisis with regard to the high price of gasoline. In the future, the crisis will take unprecedented proportions. The supply of oil will diminish and hybrid vehicles will play a major role in diffusing the situation; in comparison, electric cars are comfortable, quiet, clean and fashionable. Electric cars don't need to be cranked, a feature especially attractive to women. Ease of control is also a desirable feature. However, as shown in **Table 1**, the range is limited by energy stored in the battery. For city use, the range is adequate. After every trip, the battery requires recharging. Lead acid batteries were used in 1900. Lead acid batteries are still used in modern cars, but in electric vehicled Lithium-Ion batteries are used.

[1]Department of Electrical Engineering, BECHAR University, B.P 417 Bechar (08000) Algeria,
E-mails: gasbaoui_2009@yahoo.com; laoufi_ab@yahoo.fr; elec_allaoua2bf@yahoo.fr; nasriab1978@yahoo.fr
[2]Department of Electrical Engineering, University of E.N.S.E.T, B.P 98 ORAN (31000), Algeria,
E-mail: chakeraa@yahoo.fr

Indirectly driven EVs are powered by electric motors through vehicles propelled by in-wheel or, simply, wheel motors [1, 2]. The basic vehicle configuration of this research has two directly driven wheel motors installed and operated inside the driving wheels on a pure EV. These wheel motors can be controlled independently and have enough fast and accurate response to controls that the vehicle chassis control or motion control is more stable and robust, compared to indirectly driven EVs. Like most research on the torque distribution control of wheel motor, wheel motors [3, 14] proposed a dynamic optimal attractive force distribution control for an EV driven by four wheel motors, thereby improving vehicle handling and stability [4, 5].

Researchers assume that wheel motors are all identical with the same torque constant; neglecting motor dynamics the output torque is simply proportional to the input current with a prescribed torque constant.

To drive the motor in a wide speed range, a direct torque control system is presented. Direct torque control (DTC) is a closed-loop control technique for induction machine, which implementation is based on hysteresis comparators [3, 8, 13, 17, 18]. In this method, control variables are torque and stator flux of induction machine. This technique was initially proposed in [1, 2]. The main advantages of DTC are robust and fast torque response, no requirements for PWM pulse generation and current regulators, as well as good steady-state and dynamic performances. DTC is commonly used with a voltage source inverter (VSI), where a large electrolytic capacitor is used on the dc link of the AC/DC/AC converter in order to smooth the dc voltage and store the energy recovered from the machine during regenerative braking. Using large electrolytic capacitors is considered a disadvantage due to the short lifetime of these capacitors compared to that of ordinary capacitors and power switches, and contributing considerably to the size and weight of the converter.

The reminder of this paper is organized as follows: Section 2 reviews principle components of electric traction chain with their equations model and mechanical vehicle load modeling. Section 3 shows the development of Direct Torque controller detailed for Electric vehicle motorization. The electric differentials and the proposed structure of the studied propulsion system is given in the Section 4. Section 5 gives some simulation results of the different studied cases. Finally, the Conclusion is drawn in the latest section.

2 Electric Traction System Elements Modeling

Fig. 1 presents the general diagram of an electric traction system using an induction motor (IM) supplied by voltage inverter [4, 8].

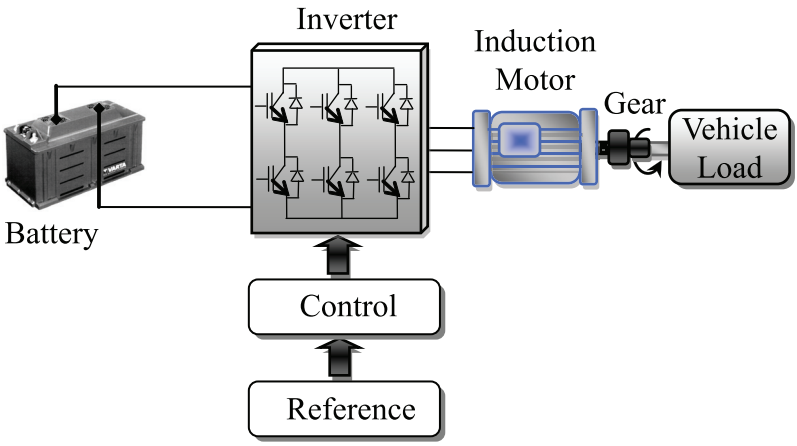

Fig. 1 − *Electrical traction chain.*

2.1 Energy source

The battery considered in this paper is of the Lithium-Ion type [5, 14]. The battery current is calculated by:

$$I_{bat} = \frac{V_{oc} - \sqrt{V_{oc}^2 - 4(R_{\text{int}} + R_t)P_b}}{2\left(R_{\text{int}} + R_t\right)}, \tag{1}$$

where P_b is output power of battery, R_{int} is internal resistance, V_{oc} is the open circuit voltage and R_t is the terminal voltage of the battery.

2.2 Static converter

In this electric traction system, we use a three balanced phases of alternating current inverter with variable frequency from the current battery [10, 14].

$$\begin{bmatrix} v_{an} \\ v_{bn} \\ v_{cn} \end{bmatrix} = \frac{U_{dc}}{2} \begin{bmatrix} 2 & -1 & -1 \\ -1 & 2 & -1 \\ -1 & -1 & 2 \end{bmatrix} \begin{bmatrix} S_a \\ S_b \\ S_c \end{bmatrix}. \tag{2}$$

S_i is logical switches obtained by comparing the control inverter signals with the modulation signal.

2.3 Traction motor

The used motorization consist of three phase induction motor (IM) supplied by a voltage inverter controlled by direct torque control. The dynamic model of three-phase, induction motor can be expressed in the stator stationery reference as [3, 6, 7, 8]:

$$\frac{\mathrm{d}}{\mathrm{d}t}\begin{cases} i_{s\alpha} = -\gamma i_{s\alpha} + \dfrac{k}{T_r}\varphi_{r\alpha} + kp\omega\varphi_{r\beta} + \dfrac{1}{\sigma L_s}v_{s\alpha}, \\ i_{s\beta} = -\gamma i_{s\beta} - kp\omega\varphi_{r\alpha} + \dfrac{k}{T_r}\varphi_{r\beta} + \dfrac{1}{\sigma L_s}v_{s\beta}, \\ \varphi_{s\alpha} = -\dfrac{L_m}{T_r}i_{s\alpha} - \dfrac{1}{T_r}\varphi_{r\alpha} - p\omega_{sl}\varphi_{r\beta}, \\ \varphi_{s\beta} = \dfrac{L_m}{T_r}i_{s\beta} + p\omega_{sl}\varphi_{r\alpha} + \dfrac{1}{T_r}v_{s\beta}, \end{cases} \tag{3}$$

where σ is the coefficient of dispersion and is given by:

$$\sigma = 1 - \frac{L_m^2}{L_s L_r}, \tag{4}$$

$$k = \frac{L_m}{\sigma L_s L_r}, \tag{5}$$

$$\gamma = \frac{R_s + R_r \dfrac{L_m^2}{L_r^2}}{\sigma L_s}, \tag{6}$$

$$T_r = \frac{L_r}{R_r}, \tag{7}$$

where L_s, L_r, L_m are the stator, rotor and mutual inductances; R_s, R_r are the stator and rotor resistances; ω_e, ω_r are the electrical and rotor angular frequency; ω_{sl} is the slip frequency; τ_r is rotor time constant; and p is the number of pole pairs.

2.4 The vehicle load

The vehicle is considered as a load characterized by many resistive torques [4, 5, 15, 16].

The vehicle inertia torque defined by the following relationship:

$$T_{in} = J_v \frac{\mathrm{d}\omega_v}{\mathrm{d}t}. \tag{8}$$

2.4.1 Aerodynamics force

This part of the force is due to the friction of the vehicle body, moving through the air. It is function of the frontal area shape protrusion such as side, mirrors, ducts and air passages spoilers and any other factor. The formula for this component is:

$$F_{aero} = \frac{1}{2}\rho A_f C_{air} v^2 . \tag{9}$$

The aerodynamics torque is:

$$T_{aero} = \frac{1}{2}\rho A_f C_{air} R_r v^2 . \tag{10}$$

2.4.2 Rolling force

The rolling resistance is caused primarily by the traction of tires on the rode. Friction in bearing and gearing systems also play their part. The rolling resistance is approximately constant, depending on the vehicle speed. It is proportional to the vehicle weight:

$$F_{tire} = Mgf_r . \tag{11}$$

The rolling torque is:

$$T_{tire} = Mgf_r R_r . \tag{12}$$

2.4.3 Hill climbing force

The force needed to drive the vehicle up a slope is the most straightforward to find. It is simply the component of the vehicle weight that acts along the slop. By simple resolution the force we see that [17].

$$F_{slope} = Mg \sin\beta . \tag{13}$$

The slope torque is:

$$T_{slope} = R_\omega Mg \sin\beta . \tag{14}$$

We obtain finally the total resistive torque:

$$T_v = T_{slope} + T_{tire} + T_{aero} . \tag{15}$$

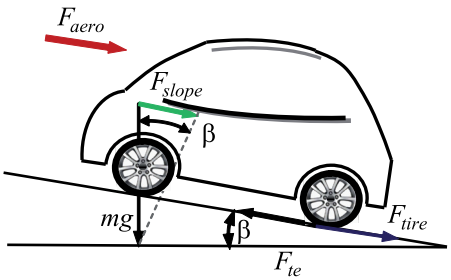

Fig. 2 − *The forces acting on vehicle moving along a slopped road.*

2.4.4 Gear

The speed gear ensures the transmission of the motor torque to the driving wheels. The gear is modeled by the gear ratio, the transmission efficiency and its inertia.

The mechanical equation is given by [11]:

$$J_e \frac{\mathrm{d}\omega_m}{\mathrm{d}t} + f\omega_m = p(T_{em} - T_r), \tag{16}$$

with:

$$T_r = \frac{1}{\eta N_{red}} T_v, \tag{17}$$

$$J_e = J + \frac{J_v}{\eta N_{red}^2}. \tag{18}$$

The modeling of the traction system allows the implementation of some controls such as the vector control and the speed control in order to ensure the globally system stability.

3 Direct Torque Control

The basic DTC strategy was developed in 1986 by Takahashi. It is based on the determination of instantaneous space vectors in each sampling period regarding desired flux and torque references. The block diagram of the original DTC strategy is shown in Fig. 3. The reference speed is compared to the measured one. The obtained error is applied to the speed regulator PI whose output provides the reference torque.

The estimated stator flux and torque are compared to the corresponding references. The errors are applied to the stator flux and torque hysteresis regulators, respectively. The outputs of the stator flux and torque regulators and the phase of the stator flux θ_s are applied to the space vector selection table block, which generates convenient combinations of the states (ON or OFF) of inverter power switches. There are eight switching combinations, two of which correspond to zero voltage space vectors which are (000) and (111). The stator flux φ_s is controlled by a tow-level hysteresis regulator, where the logical function c_φ takes "+1" to increase φ_s and "–1" to decrease it. The electro-magnetic torque T_{em} is controlled by its hysteresis regulator, where the logical function $c_{T_{em}}$ gives not only the states "+1" and "–1" (increase/decrease), but also "0" to hold T_{em} [3, 7, 8, 13, 17, 18].

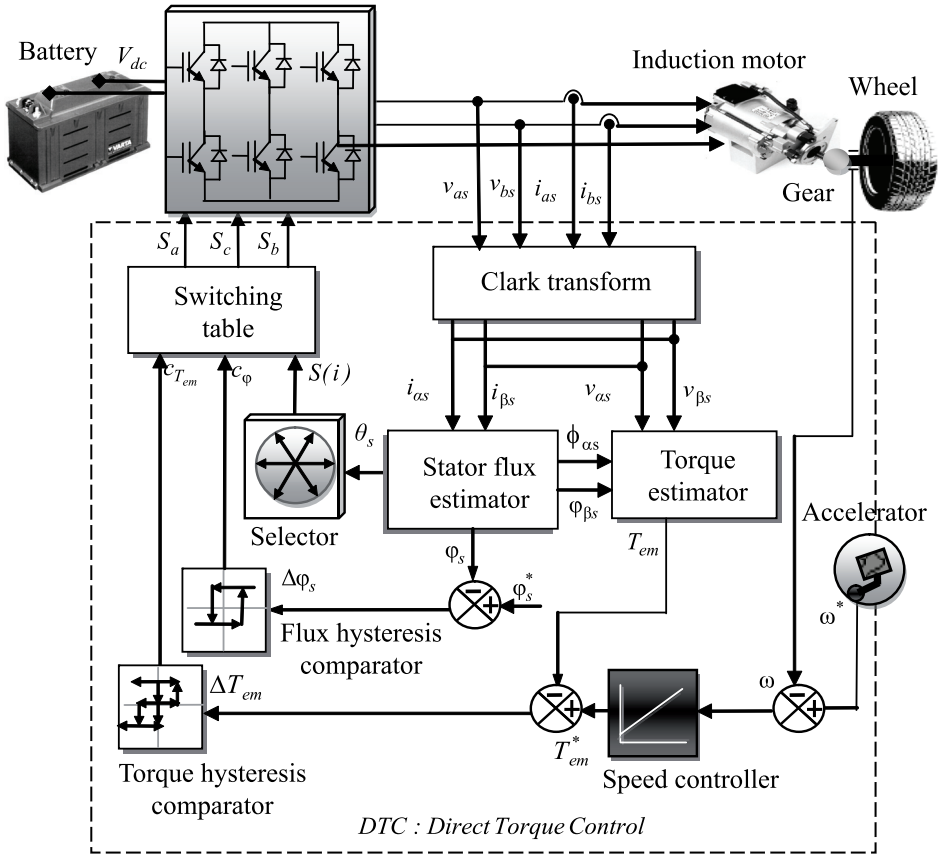

Fig. 3 − *Bloc diagram of* DTC *for an* EV *induction motor.*

The estimation value of flux and its phase angle is calculated in expression:

$$\begin{cases} \varphi_{s\alpha} = \int_0^t (V_s - R_s i_{s\alpha})\,\mathrm{d}t, \\ \varphi_{s\beta} = \int_0^t (V_s - R_s i_{\beta\alpha})\,\mathrm{d}t, \end{cases} \tag{19}$$

$$\varphi_{s\alpha} = \sqrt{\varphi_{s\alpha}^2 + \varphi_{s\beta}^2}, \quad \theta_s = \arctan\left(\frac{\varphi_{s\beta}}{\varphi_{s\alpha}}\right), \tag{20}$$

$$T_{em} = \frac{3}{2} p(\varphi_{s\alpha} i_{s\beta} - \varphi_{s\beta} i_{s\alpha}). \tag{21}$$

The torque is controlled by three-level Hysteresis. Its estimation value is calculated by expression (21).

In this part we precise the important of the differential electronic as a good technological solution for the modern electric vehicle speed computation.

4 Electric Differentials Speed Computation

The proposed control system principle could be summarized as follows:

Speed network control is used to control each motor torque. The speed of each rear wheel is controlled using speed difference feedback. Since the two rear wheels are directly driven by two separate motors, the speed of the outer wheel will need to be higher than the speed of the inner wheel during steering maneuvers (and vice-versa). This condition can be easily met if the speed estimator is used to sense the angular speed of the steering wheel. The common reference speed ω_{ref} is then set by the accelerator pedal command. The actual reference speed for the left drive ω^*_{left} and the right drive ω^*_{right} are then obtained by adjusting the common reference speed ω^* using the output signal from the DTC speed estimator. If the vehicle is turning right, the left wheel speed is increased and the right wheel speed remains equal to the common reference speed ω^*. If the vehicle is turning left, the right wheel speed is increased and the left wheel speed remains equal to the common reference speed ω^* [7, 9, 10]. Usually, a driving trajectory is adequate for an analysis of the vehicle system model.

From the mode show in Fig. 6, the following characteristic can be calculated:

$$R = \frac{L_w}{\tan\delta}, \tag{22}$$

where δ is the steering angle. Therefore, the linear speed of each wheel drive is given by:

$$\begin{cases} V_1 = \omega_v (R - d_\omega/2), \\ V_2 = \omega_v (R - d_\omega/2), \end{cases} \tag{23}$$

and their angular speed by:

$$\begin{aligned} \omega^*_{mr} &= \frac{L_\omega - (d_\omega/2)\tan\delta}{L_w}\omega_{mr}, \\ \omega^*_{ml} &= \frac{L_\omega - (d_\omega/2)\tan\delta}{L_w}\omega_{lm}, \end{aligned} \tag{24}$$

where ω_v is the vehicle angular speed according to the center of turn.

The difference between wheel drive angular speeds is then:

$$\Delta\omega = \omega_{rm}^* - \omega_{lm}^* = \frac{d_\omega \tan\delta}{2L_\omega}\omega_v \,. \tag{25}$$

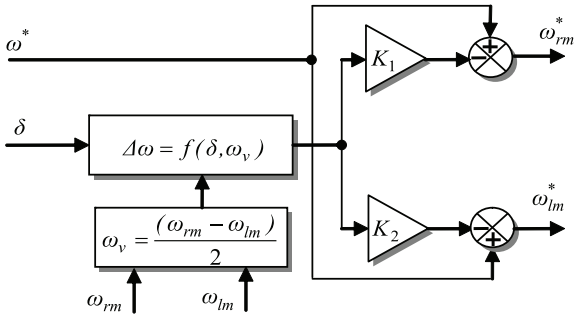

Fig. 4 − *Block diagram of the differential system.*

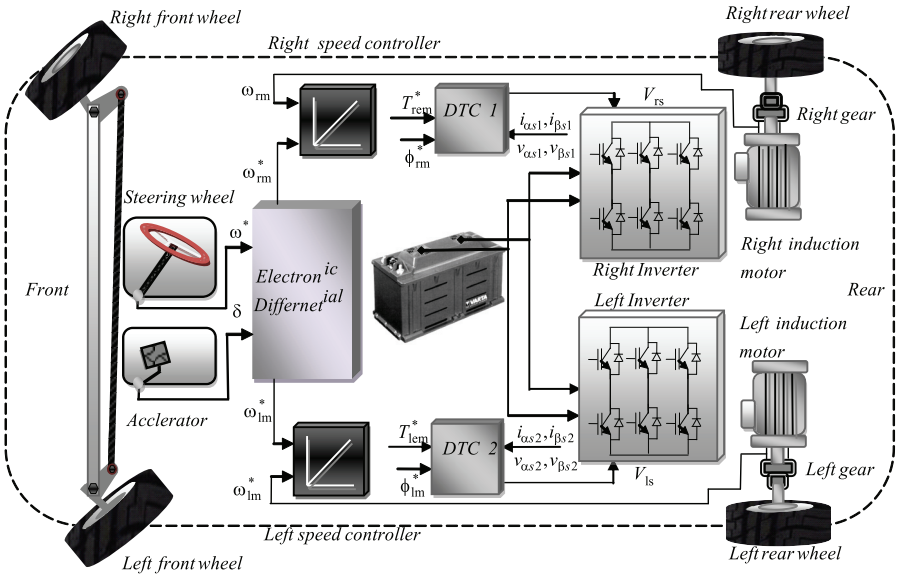

Fig. 5 − *Driving wheels control system.*

And the steering angle indicates the trajectory direction is:

$$\delta > 0 \quad \Rightarrow \quad Turn\ left, \tag{26}$$

$$\delta = 0 \quad \Rightarrow \quad Straight\ ahead, \tag{27}$$

$$\delta < 0 \quad \Rightarrow \quad Turn\ right. \tag{28}$$

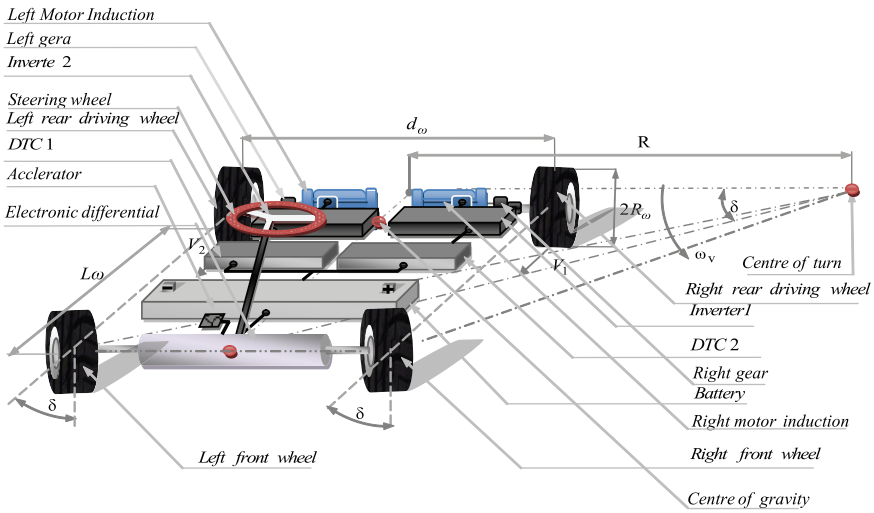

Fig. 6 – *Structure of Vehicle in Curve.*

5 Results and Discussion

In order to characterize the driving wheel system behavior, simulations were carried using the model of Fig. 5.

Case A: Curved road.

Curved road at right side with speed of 80 km/h at time 2.5 s and in the left side at 4 s.

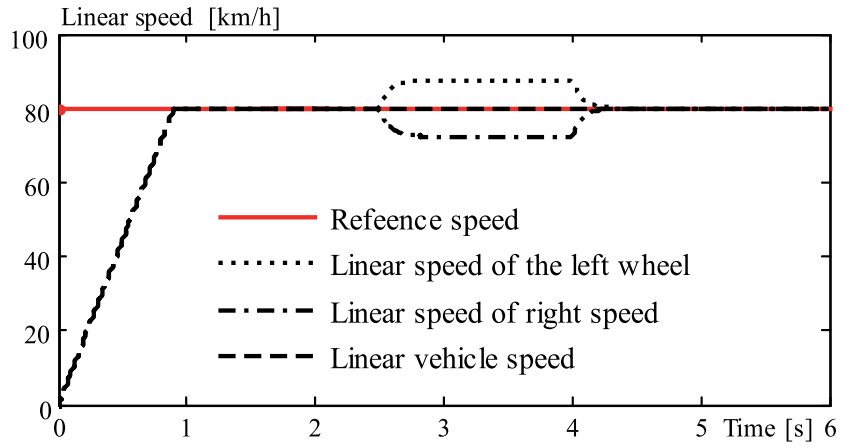

Fig. 7 – *Linear speeds.*

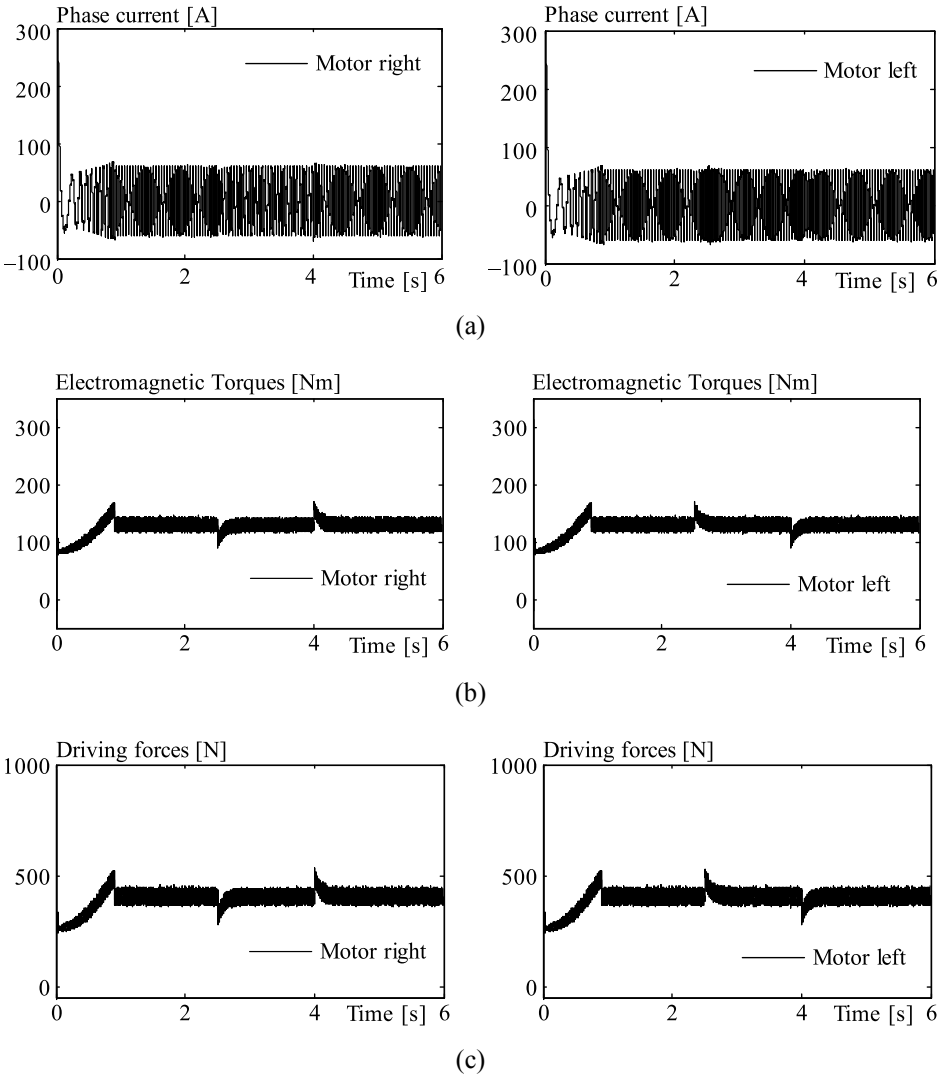

Fig. 8 − (a) *Phase currents for the right and left*;
(b) *Electromagnetic torques for the right and left motor*;
(c) *Driving forces for the left and right motor.*

– At $t = 2.5\text{s}$ the vehicle driver turns the steering wheel on a curved road at the right side with 80 km/h speed, the assumption is that the two motors are not disturbed. In this case the driving wheels follow different paths, and they turn in the same direction but with different speeds. The electronic

differential acts on the two motor speeds by decreasing the speed of the driving wheel on the right side situated inside the curve, and on the other hand by increasing the wheel motor speed in the external side of the curve. The behavior of these speeds are given by Fig. 7. The DTC controller act immediately on the torque speed loop's and rejects the disturbance of the speed response and gives more and more efficiency to the electronic differential output references At $t = 4\text{s}$ the vehicle situated in the second curve but in the left side the electronic differential compute the novel steering wheels speeds references in order to stabilize the vehicle inside the curve. Once this speeds are computed the efforts demand on the two back motors increase and it's explain by the shame of Fig. 7 the driving forces developed satisfy the traction chain demand by the way the vehicle weigh inertia doesn't have effect on the developed torque control model the figures which explain the curve road situations are illustrated by Fig. 8.

Case B: Straight road with 10% slope at 2.5s < *t* < 4s.

– At $4\text{s} < t < 6\text{s}$, the EV are driving in straight road, this test explain the effect of the slope on the EV. The driving wheels linear speeds stay the same and the road drop does not influence the torque control of each wheels. The both of the back motors develop more and more electromagnetic torque for passing the slope. The behavior of these speeds is given by Fig. 9. The variation of Electromagnetic torques and driving forces are illustrated in Figs. 10b and 10c. The presence of slope causes a large increase in the phase current for the right and left motor, The two motors absorb more energy which explain by the Fig. 10a. The current demand increases and the vehicle can pass the slope easily.

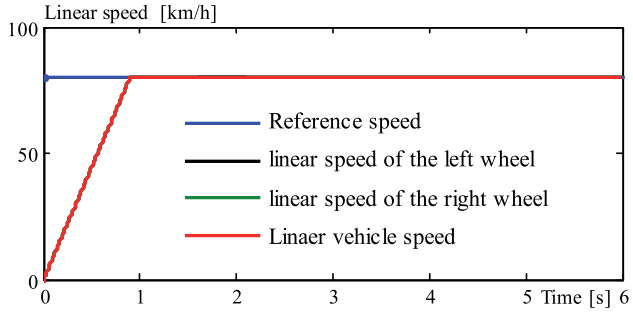

Fig. 9 – *Linear speeds.*

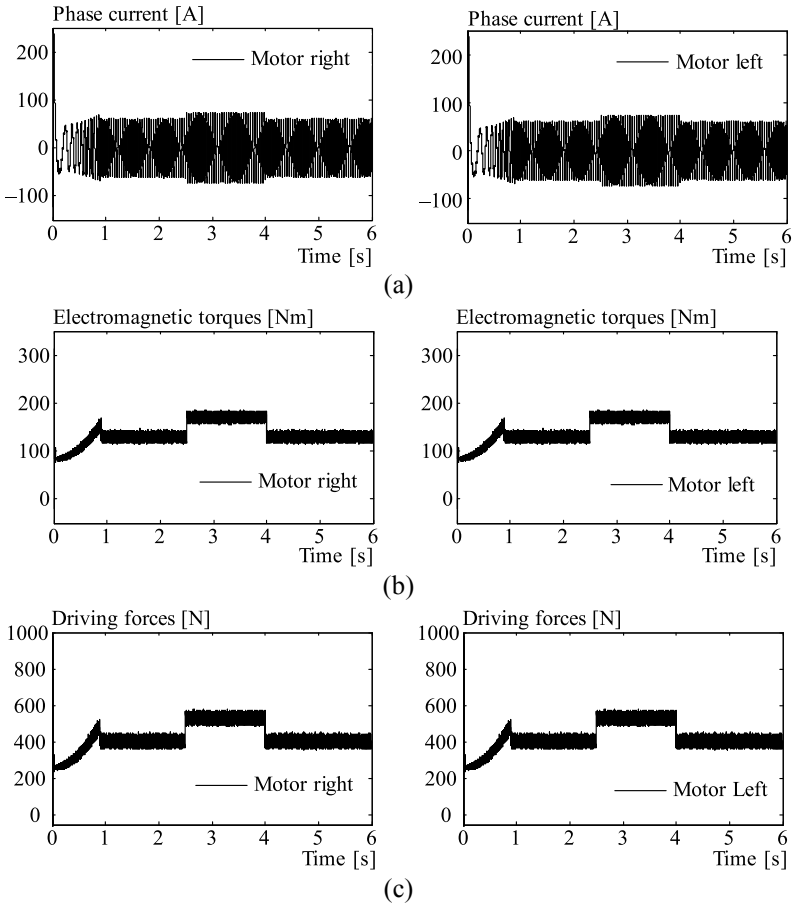

Fig. 10 – (a) *Phase currents for the right and the left motor*; (b) *Electromagnetic torques for the right and the left motor*; (c) *Driving forces for the right and the left motor.*

Case C: Descent slopped road of –10% at 2.5s < *t* < 4s.

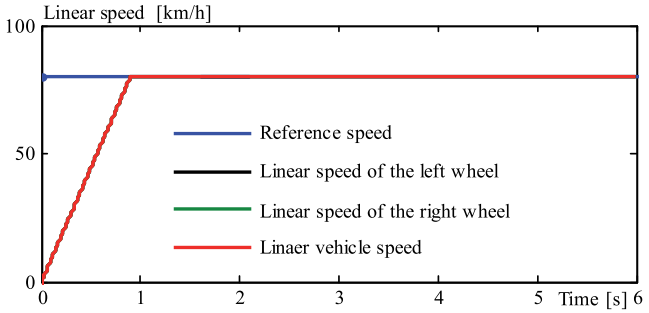

Fig. 11 – *Linear speeds.*

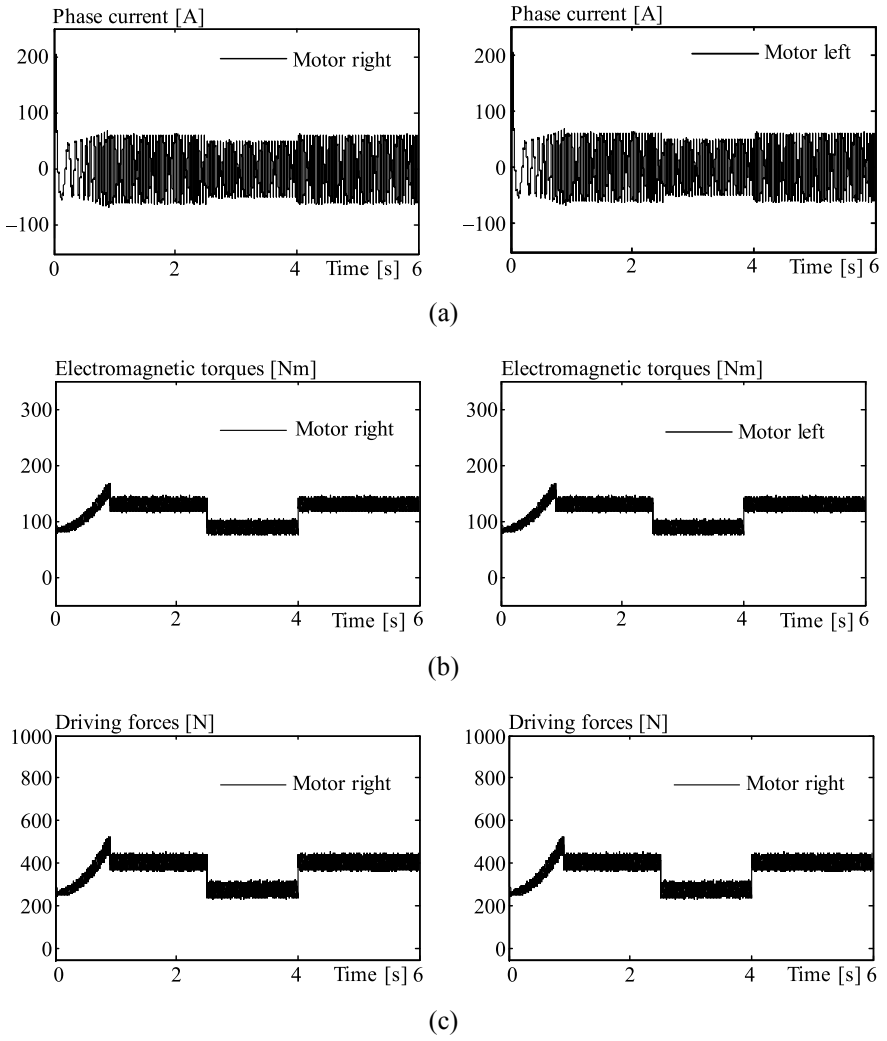

Fig. 12 – (a) *Phase current of the right and the left motor*;
(b) *Electromagnetic torques for the right and left motor*;
(c) *Driving forces for the left and right motor.*

– This test clarifies the effect of the descent slope on the electric vehicle moving on straight road. The linear speed response is illustrated in Fig. 11. The presence of descent causes a great decrease in the phase current of each motor by means that the aerodynamic force became an motor force and the other resistive torques became motor torque and the kinetic energy given to

the vehicle help the battery in order to charge the empty battery cells these results of test are shown in Figs. 12a. The motor absorbed the half of the slopped energy.

In order to show the effect of disturbance on the vehicle speed using DTC controller. The EV is submitted with constant speed 80 km/h in straight way during simulation and the results obtained are compared with other results given in the literature [11]. We can summaries the vehicle speed results in the **Table 1**.

Table 1
Performance of DTC *in the speed response* 2s < *t* < 6s.

Results	Rising time [s]	Overshoot [%]	Steady state error [%]
DTC controller	0.7390	0.0023	0.0000

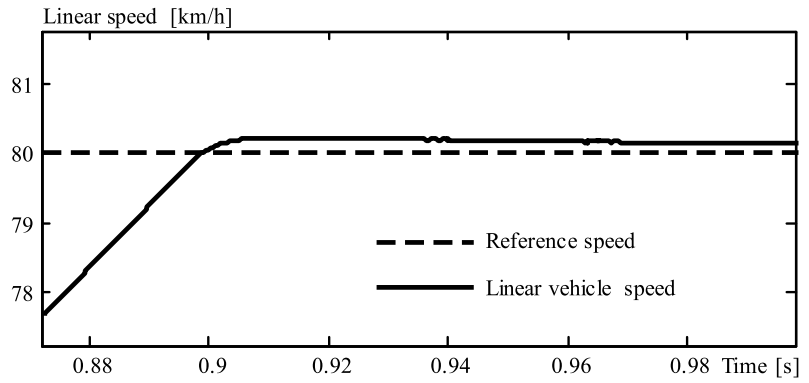

Fig. 13 − *Zoomed of linear speeds.*

From Fig. 13 and **Table 1** we can say that the effect of disturbance is neglected in the DTC controller. It appears clearly that the DTC controller is easy to apply compared with classical PI speed controller and give satisfactory and good dynamical performances results more than the classical one, that reason of the DTC uses in electric vehicle propulsion in medium and low speed regions.

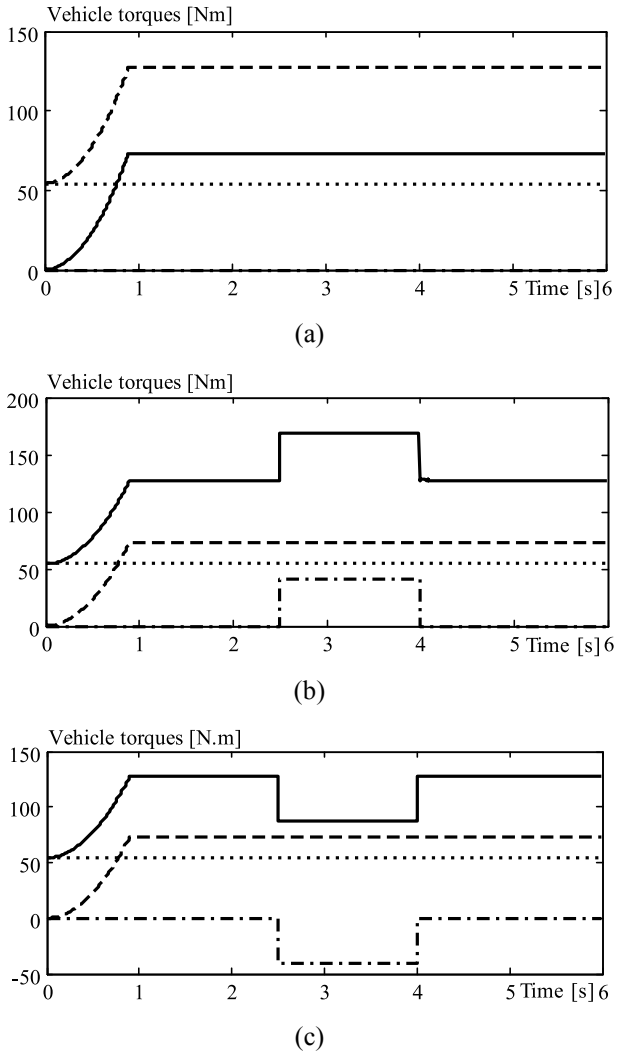

Fig. 14 − *Vehicle torques for different cases*, (a) Case A, (b) Case B, (c) Case C.

The globally motor torque developed by EV is 235 Nm. Fig. 14 gives the maximum vehicle torque in each of the cases and the comparative studies are shown in **Table 2**, for each **Case A**, **B** and **C**.

According to the formulas (10), (12) and (14) and Fig. 14, the variation of vehicle torque in different cases is shown in Fig. 15. The vehicle torque develops 127.73 Nm in the first case in order to pass the curve.

Table 2
Variation of vehicle torque in different paths at 2s < *t* < 6s.

Cases	Case A	Case B	Case C
Vehicle torque [Nm]	127,37	169.00	86.99
Percentage of the vehicle torque compared with motor torque [%]	54.365	71.91	37.01

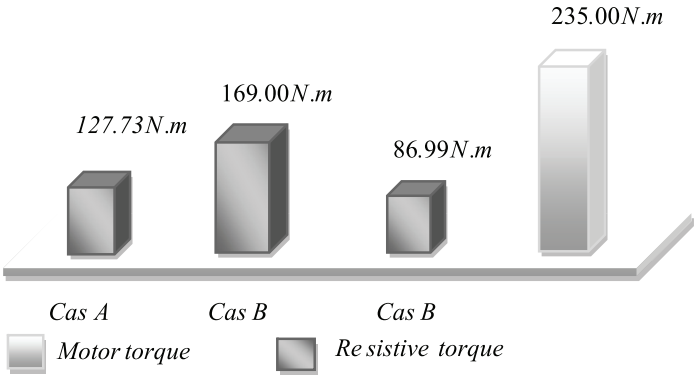

Fig. 15 − *Variation of vehicle torques in different cases.*

In the second case (**Case B**: acceleration phase's) the electromagnetic torque go up 127.73 Nm to 169 Nm that present amount of 71.91% of the total nominal motor torque 237 Nm. This variation make clear the slope torque effect's on the traction chain in the last case a great decreases for electromagnetic torque around 50% of the slope torque (deceleration phase's when the battery is in the recharge state) .the resistive torque of the **Case C** present 37.01% of globally nominal motor torque. The result prove that the traction chain under slope constraint develop the double effort comparing with the inverse slope case by means that the vehicle needs the half of its energy in the deceleration phase's compared with the acceleration one's.

6 Conclusion

The research outlined in this paper has demonstrated the feasibility of an improved vehicle stability which utilizes two independent back drive wheels for motion by using the direct torque control. This paper proposes an independent machine control structure applied to a propulsion system ensuring by the electronic differential. The estimation of torque and stator flux was compared

with torque and flux desired using the hysteresis comparator models. The estimation error was reduced and robustness was enhanced. It is proved that fast torque response can be obtained by simulation. The direct torque control models improve the driving wheels speeds control with high accuracy in curved road or in slopped ones. The disturbances do not affect the performances of the driving motors in the other hand the proposed control gives good dynamic characteristics of the traction chain.

7 Appendix

Table 3
Vehicle Parameters.

T_{em}	Motor traction torque	238 Nm
J_e	Moment on inertia of the drive train	7.07 kgm^2
R_w	Wheel radius	0.32 m
η	Total transmission efficiency	0.93
M	Vehicle mass	1300 kg
f_r	Bearing friction coefficient	0.32
C_{air}	Aerodynamic coefficient	0.32
A_f	Vehicle frontal area	2.60 m^2
f_v	Vehicle friction coefficient	0.01
L_w	Distance between two wheels and axes	2.5 m
d_w	Distance between the back and the front wheel	1.5 m

Table 4
Induction Motors Parameters.

R_r	Rotor winding resistance (per phase)	0.0503 Ω
R_s	Stator winding resistance (per phase)	0.08233 Ω
L_s	Stator leakage inductance (per phase)	724 μH
L_m	Magnetizing inductance (per phase)	0.0151 H
L_r	Rotor leakage inductance (per phase)	724 μH
f_c	Friction coefficient	0.02711
P	Number of poles	4

Table 5
Symbols, Designation and Units.

Symbols	Nomenclature	Units
J	Rotor inertia	kg m^2
J_e	Moment of inertia of the drive train	kg m^2
J_v	Vehicle inertia	kg m^2
T_{em}	Electromagnetic torque	Nm
T_v	Vehicle torque	Nm
T_{slope}	Slope torque	Nm
T_{aero}	Aerodynamic torque	Nm
T_{tire}	Tire torque	Nm
η	Transmission efficiency	%
L_w	Distance between two wheels	m
d_w	Distance between the back and the front wheel	m
R	Curve radius	m
V_{dc}	Battery voltage	V
$\Delta\omega_v$	Angular speed variation given by electronic differential	rad/s
ω_{rm}	Right wheel angular speed	rad/s
ω_{lm}	Left wheel angular speed	rad/s
ω^*_{rm}	Right wheel angular speed of reference	rad/s
ω^*_{lm}	Left wheel angular speed of reference	rad
δ	Reel angle wheel curve's	rad

8 References

[1] Y.P. Yang, C.P. Lo: Current Distribution Control of Dual Directly Driven Wheel Motors for Electric Vehicles, Control Engineering Practice, Vol. 16, No. 11, Nov. 2008, pp. 1285 – 1292.

[2] P. He, Y. Hori, M. Kamachi, K. Walters, H. Yoshida: Future Motion Control to be Realized by In-wheel Motored Electric Vehicle, 31st Annual Conference of the IEE Industrial Electronics Society, Raleigh, North Carolina, USA, 2005, pp. 2632 – 2637.

[3] J.K. Kang, S.K. Sul: New Direct Torque Control of Induction Motor for Minimum Torque Ripple and Constant Switching Frequency, IEEE Transaction on Industrial Application, Vol. 35, No. 5, Sept/Oct. 1999, pp. 1076 – 1082.

[4] C.C. Chan, Y.S. Wong: Electric Vehicles Charge Forward, IEEE Power and Energy Magazine, Vol. 2, No. 6, Nov/Dec. 2004, pp. 24 – 33.

[5] Z.Q. Zhu, D. Howe: Electrical Machines and Drives for Electric, Hybrid, and Fuel Cell Vehicles, Proceeding of the IEEE, Vol. 95, No. 4, April 2007, pp. 746 – 765.

[6] P. Vas: Sensorless Vector and Direct Torque Control, Oxford University Press, NY, 1998.

[7] K. Itoh, H. Kubota: Thrust Ripple Reduction of Linear Induction Motor with Direct Torque Control, International Conference on Electrical Machines and Systems, Nanjing, China, Vol. 1, Sept. 2005, pp. 655 – 658.

[8] L. Chen, K.L. Fang: A Novel Direct Torque Control for Dual-three-phase Induction Motor, International Conference on Machine Learning and Cybernetics, Xian, China, Vol. 2, Nov. 2003, pp. 876 – 881.

[9] A. Schell, H. Peng, D. Tran, E. Stamos, C.C. Lin, M.J. Kim: Modeling and Control Strategy Development for Fuel Cell Electric Vehicle, Annual Reviews in Control, Vol. 29, No. 1, 2005, pp. 159 – 168.

[10] A. Haddoun, M.E.H. Benbouzid, D. Diallo, R. Abdessemed, J. Ghouili, K. Srairi : Modeling, Analysis and Neural Network Control of an EV Electrical Differential, IEEE Transaction on Industrial Electronic Vol. 55, No. 6, June 2008, pp. 2286 – 2294.

[11] A. Nasri, A .Hazzab, I.K. Bousserhane, S. Hadjeri, P. Sicard: Two Wheel Speed Robust Sliding Mode Control for Electric Vehicle Drive, Serbian Journal of Electrical Engineering , Vol. 5, No. 2, May 2008, pp. 199 – 216.

[12] K. Hartani, M. Bourahla, Y. Miloud, M. Sekour: Electronic Differential with Direct Torque Fuzzy Control for Vehicle Propulsion System, Turkish Journal of Electrical Engineering and Computer Sciences, Vol. 17, No. 1, 2009, pp. 21 – 38.

[13] L.T. Lam, R. Louey: Developpement of Ultra-battery for Hybrid-electric Vehicle Applications, Journal of Power Sources, Vol. 158, No. 2, Aug. 2006, pp. 1140 – 1148.

[14] J. Larminie: Electric Vehicle Technology Explained, John Wiley and Sons, NJ, 2003.

[15] A. Haddoun, M.E.H. Benbouzid, D. Diallo, R. Abdessemed, J. Ghouili, K. Srairi: Analysis, Modeling and Neural Network Traction Control of an Electric Vehicle without Differential Gears, International Conference Electric Machines and Drives, Antalya, Turkey, May 2007, pp. 854 – 859.

[16] M. Vasudevan, R. Arumugam: New Direct Torque Control Scheme of Induction Motor for Electric Vehicles, Asian Control Conference, Melbourne, Australia, Vol. 2, July 2004, pp. 1377 – 1383.

[17] M.E.H. Benbouzid, D. Diallo, M. Zeraoulia: Advanced Fault-tolerant Control of Induction Motor Drives for EV/HEV Traction Applications: From Conventional to Modern and Intelligent Control Techniques, IEEE Transaction on Vehicular Technology, Vol. 56, No. 2, March 2007, pp. 519 – 528.

[18] A. Arif, A. Betka, A. Guettaf: Improvement the DTC System for Electric Vehicles Induction Motors, Serbian Journal of Electrical Engineering, Vol. 7, No. 2, Nov. 2010, pp. 149 – 165.